ACS APPLIED MATERIALS & INTERFACES

Research Article

www.acsami.org

Cleavable PEGylation and Hydrophobic Histidylation of Polylysine for siRNA Delivery and Tumor Gene Therapy

Haiyan Zhu,[†,‡,∥] Chunyan Dong,[‡,∥] Haiqing Dong,[‡] Tianbin Ren,[‡,§] Xuejun Wen,[§] Jiansheng Su,*[,†] and Yongyong Li*[,‡]

[†]Laboratory of Oral Biomedical Science and Translational Medicine, Department of Prosthodontics, School of Stomatology, Tongji University, Shanghai, China

[‡]Shanghai East Hospital, The Institute for Biomedical Engineering and Nano Science (iNANO), Tongji University School of Medicine, Shanghai, China

[§]The Institute for Engineering and Medicine (IEM), Virginia Commonwealth University, Richmond, Virginia 23284, United States

Supporting Information

ABSTRACT: Polylysine with cleavable PEGylation and hydrophobic histidylation (mPEG-SS-Lys$_n$-r-His$_m$) was designed and developed for efficient siRNA delivery and tumor therapy. mPEG-SS-Lys$_n$-r-His$_m$ was used to carry and deliver small interfering RNA (siRNA) for silencing endogenous vascular endothelial growth factor (VEGF) expression and inhibiting tumor growth in HepG2 tumor-bearing mice. In this gene vector, histidine(Bzl) was selected for hydrophobic histidylation for the proton sponge ability of the imidazole ring and hydrophobic benzyl group. Cleavable PEGylation was introduced for in vivo circulation as well as selective PEG detachment in response to intracellular reduction condition in order to release the genetic payload. PEG detachment induced gene release was supported by agarose gel electrophoresis retardation assay, undertaken in the intracellular relevant reduction condition. In vitro transfection evaluation of histidylated copolymers, using pEGFP as genetic model, indicated significantly higher GFP expression than unmodified counterparts, comparable to the gold standard PEI. The efficacy of hydrophobic histidylation was found to be pronounced in mesenchymal stem cells (MSCs). In vivo application of the VEGF-siRNA package by tailored mPEG-SS-Lys$_n$-r-His$_m$ showed distinct tumor suppression in terms of macroscopic tumor volume and molecular analysis.

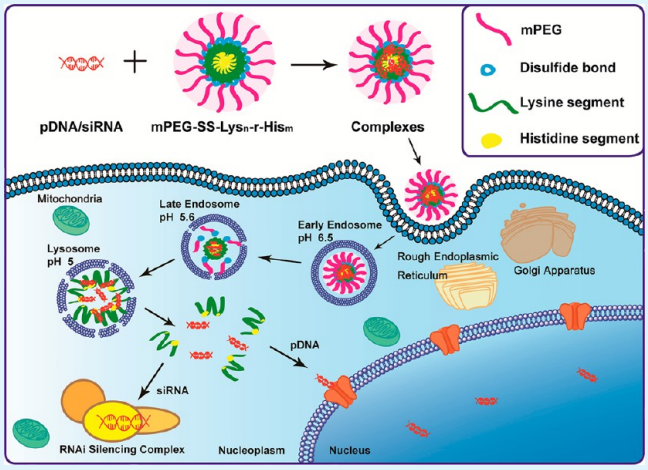

KEYWORDS: *gene therapy, RNA interference, MSCs, disulfide bond, histidine(Bzl)*

INTRODUCTION

Gene therapy has emerged as a promising tool for cancer treatment. Gene vector with ideal properties of plasmid and RNA deliveries is generally required for gene package protection and transport to site of interest.[1,2] Considering biosafety of the viral gene vector, nonviral vector is highly preferred as a promising alternative for its straightforward production, relatively bioinert, respectable gene loading capacity, and easy bioconjugation.[3,4] Gene navigation to a specific lesion includes extracellular (packing of nucleic acids, long circulation, and targeted site delivery) and intracellular barriers (cellular uptake, endolysosome escape, and nuclear import).[5] Sufficient circulation time and selective intracellular unpackage represent two pivotal parameters to determine gene transfection efficiency.

PEGylation of gene vector has been one of the most employed methods to extend in vivo circulation time of genetic payload. It exhibits considerable resistance to undesired aggregation and unspecific interactions with serum proteins during in vivo circulation.[4] However, permanent PEGylation will prevent the gene vector from intimate interaction with cell membrane as well as the subsequent intracellular release of gene. In our previous works,[6,7] we have developed cleavable PEGylation in order to meet specific requirements in gene delivery. The key advantage of this strategy is to incorporate disulfide bond between the PEG segment and gene vector (generally cationer chains). Disulfide bond will be selectively cleaved in tumor- (several times higher than normal condition) under relevant intracellular-(hundred times higher than extracellular) reduction condition. This mechanism can cause

Received: March 30, 2014
Accepted: June 3, 2014
Published: June 3, 2014

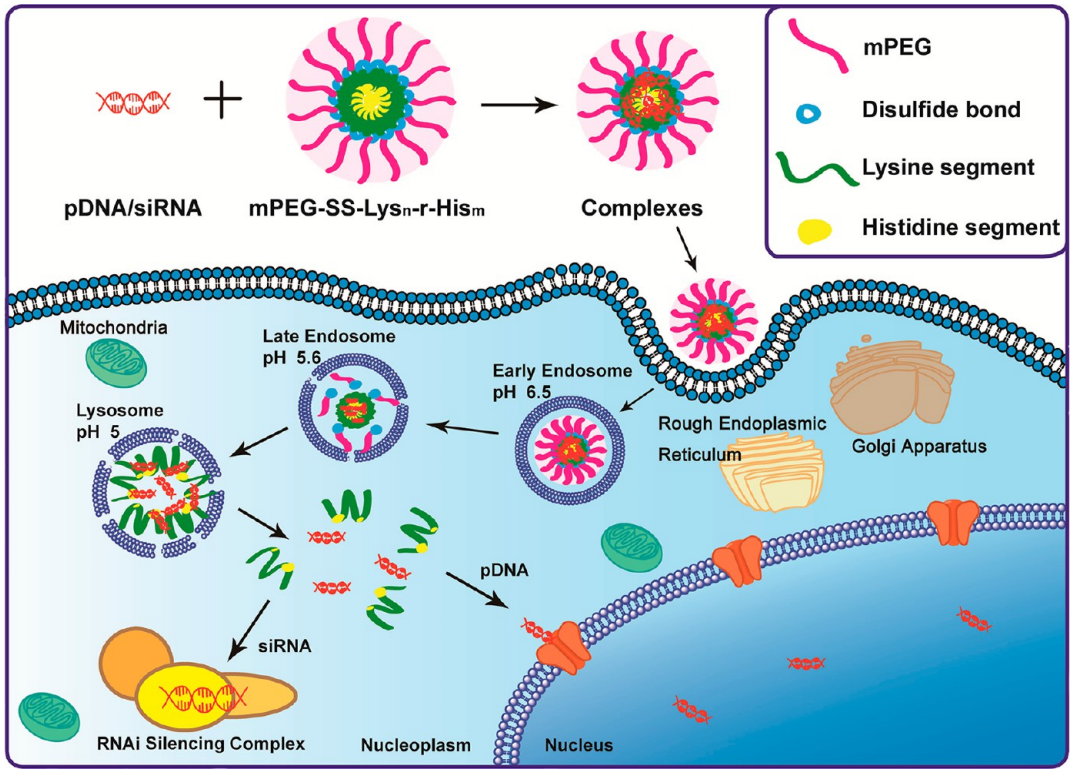

Figure 1. Fabrication and different intracellular processes of pDNA and siRNA complexes.

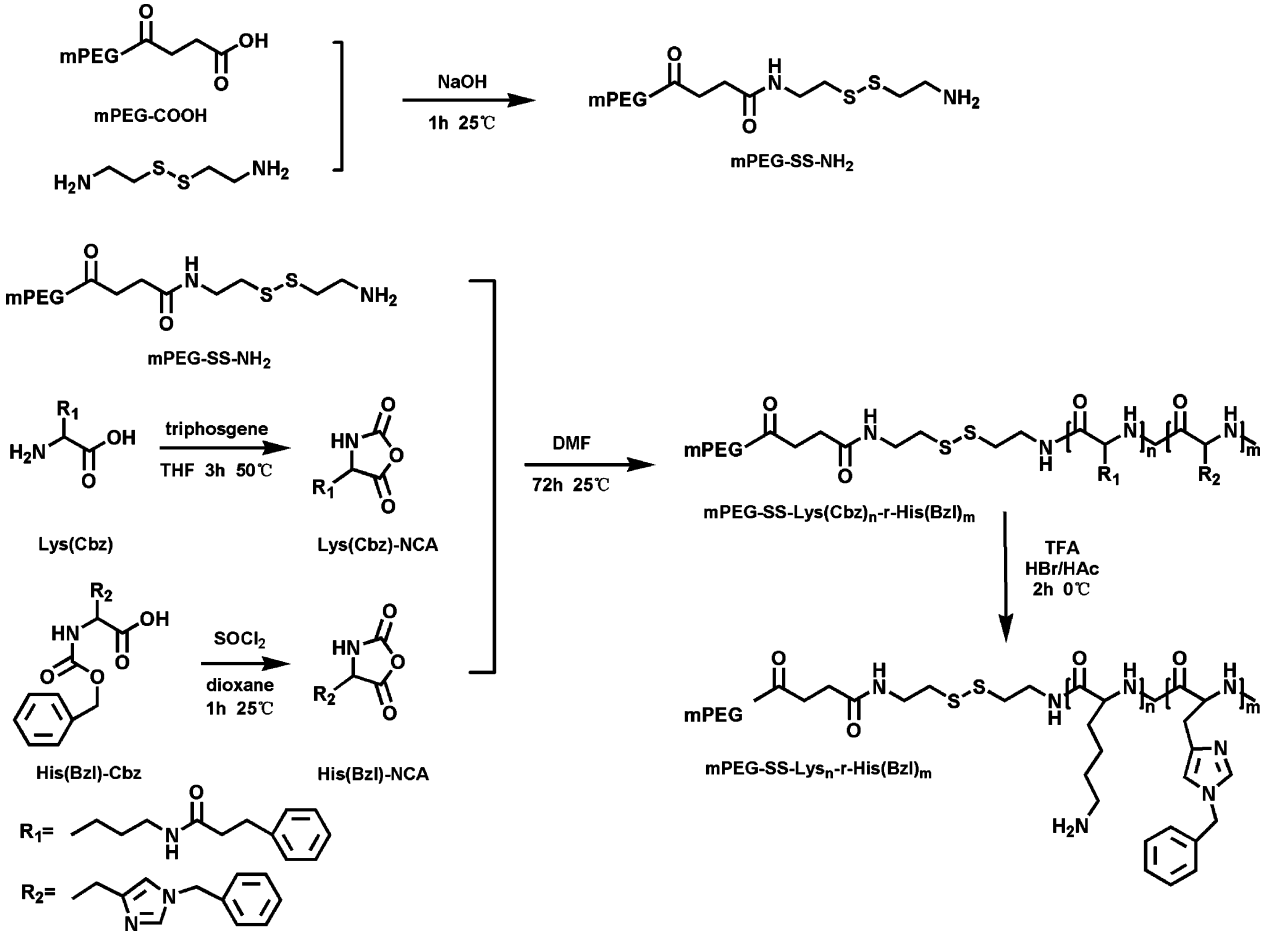

Figure 2. Synthesis of mPEG-SS-Lys$_n$-r-His(Bzl)$_m$.

dx.doi.org/10.1021/am501928p | ACS Appl. Mater. Interfaces 2014, 6, 10393−10407

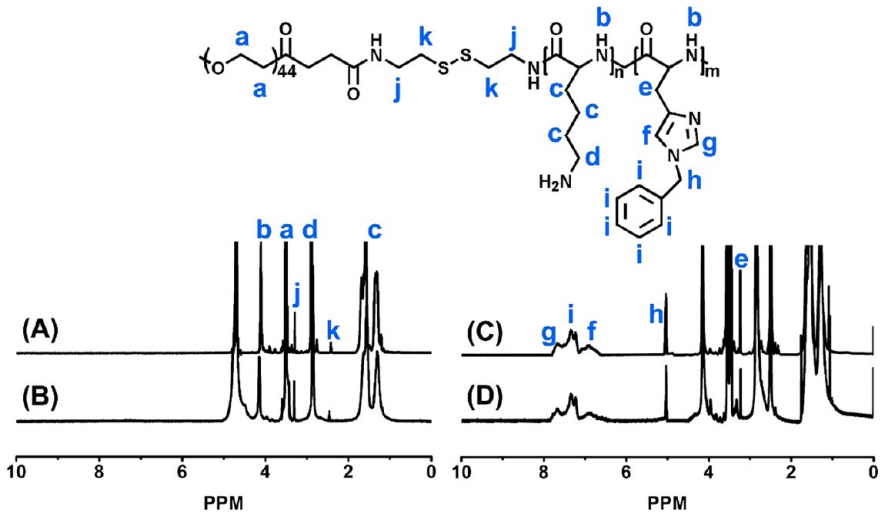

Figure 3. ^{1}H NMR spectra of (A) mPEG-SS-Lys$_{55}$, (B) mPEG-SS-Lys$_{95}$, (C) mPEG-SS-Lys$_{55}$-r-His$_{20}$, and (D) mPEG-SS-Lys$_{95}$-r-His$_{20}$.

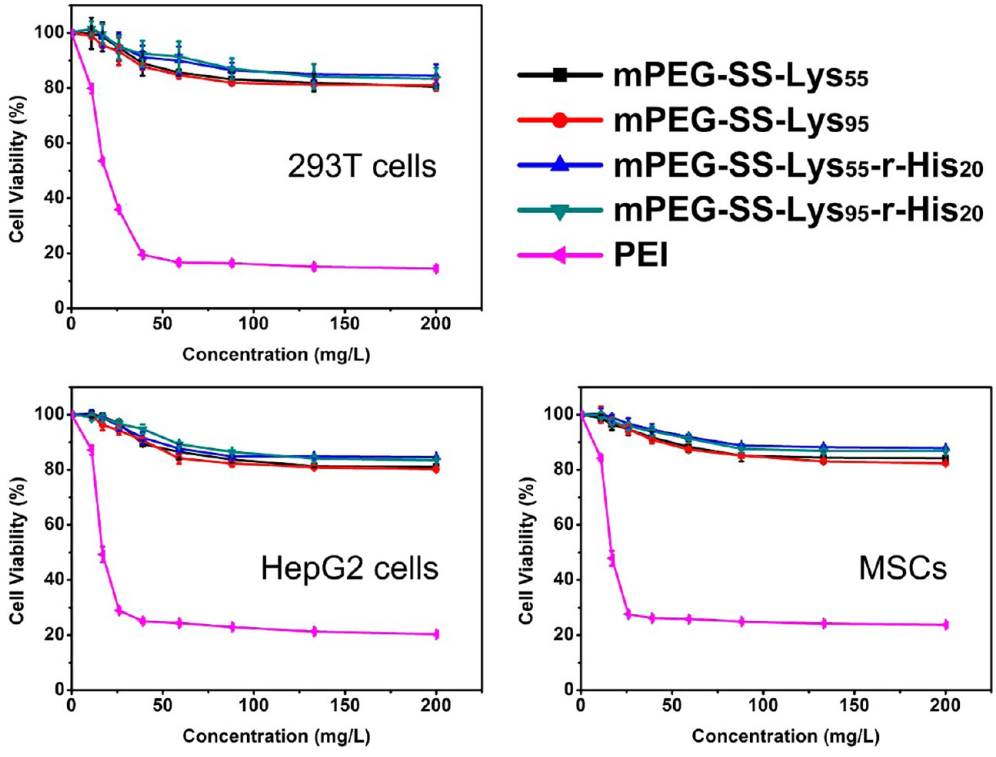

Figure 4. Cytotoxicity of mPEG-SS-Lys$_n$-r-His$_m$ in 293T cells, HepG2 cells, and MSCs at various concentrations for 24 h. Data are shown as mean ± SD (n = 5).

detachment of PEG segment thus promoting interaction with cell membrane and intracellular release. It was found that this unique design can significantly improve the gene transfection efficiency compared to the control experiment with permanent linkage.

siRNA has been recognized as one of powerful biotherapeutics for gene therapy as the on-site action is located in cytoplasm, avoiding the process of nucleus entry.[8] It has been found, however, that siRNA was prone to be fast degraded by ubiquitous RNases in both assembly process and in vivo circulation.[9] Moreover, in comparison with DNA, siRNA carries much less phosphate groups for its short sequence, which usually provides insufficient electrostatic interaction with gene vector.[5] For an efficient siRNA assembly, hydrophobic interaction has been incorporated into gene vector in order to provide a "phase separation" in a single gene/vector nanocomplex.[10] This phase separation can lead to strong compactness and reduction of siRNA leakage compared with other strategies.[11] Meanwhile, histidylation of gene vector has been shown to maintain being protonized,[12] resulting in endolysosome escape which prevents enzymatic degradation of nucleic acids. This will in tern effectively enhance transfection efficiency.

In this study, we report an efficient siRNA delivery vector, polylysine with cleavable PEGylation and hydrophobic histidylation, as shown in Figure 1. This system meets the requirements for gene delivery in vitro and in vivo. Hydrophobic histidylation is specifically designed for simultaneously

stabilizing siRNA complexes via hydrophobic interaction, which is critical for siRNA delivery. Histidylation of polylysine endows the copolymers proton buffering capacity for endolysosome escape. PEG-shell can be detached via disulfide bond cleavage in cells to meet the conflict requirements of PEG inside and outside cells. The physicochemical properties, biosafety, transfection efficiency in vitro, biodistribution, and tumor gene therapy in vivo were investigated.

RESULTS AND DISCUSSION

Synthesis and Characteristics of mPEG-SS-Lys$_n$-r-His$_m$. To construct an effective gene delivery vector for both pDNA and siRNA, mPEG-SS-Lys$_n$-r-His$_m$ catiomer with disulfide-linked PEGylation and hydrophobic histidylation was designed and developed. mPEG-SS-Lys$_n$ was synthesized as control. The redox cleavable disulfide bond affords selective mPEG cleavage, while hydrophobic histidine(Bzl) enables remarkable endolysosome escape and ensures siRNA stability. In this study, mPEG-SS-Lys$_n$-r-His$_m$ copolymers were synthesized by the ring-opening polymerization of Lys(Cbz)-NCA and His(Bzl)-NCA with mPEG-SS-NH$_2$ as an initiator. The synthesis protocol of the multifaceted copolymers is illustrated in Figure 2.

After exhausted purification, the final productions were characterized by ^{1}H NMR spectroscopy. As shown in Figure 3, the peaks at 3.56 and 5.03 ppm are assigned to $-CH_2$ in mPEG segment and $-CH_2$ in benzyl moiety, respectively. By integration of the peaks in Figure 3, the n and m values in each copolymer can be calculated and the copolymers are described as mPEG-SS-Lys$_{55}$, mPEG-SS-Lys$_{95}$, mPEG-SS-Lys$_{55}$-r-His$_{20}$, and mPEG-SS-Lys$_{95}$-r-His$_{20}$. MTT assays showed that these four copolymers exhibited acceptable cytotoxicity in 293T cells, HepG2 cells, and MSCs (Figure 4), which was an important precondition for cellular and in vivo tests.

Buffering Capacity. For structural stability and buffering ability needed for siRNA, histidine(Bzl) unit was selected in this study. It has been shown that the imidazole group of histidine possesses the proton sponge effect in the endolysosomal pH range and improves the transfection efficiency via promoting gene escaping into cytoplasm.[13] Recent studies indicated that the imidazole group of carboxymethyl poly(L-histidine), as a new pH-sensitive polypeptide, can be protonated at endolysosomal pH (<6).[14,15] The buffering ability of mPEG-SS-Lys$_n$-r-His$_m$ copolymers was verified by the acid–base titration profiles (Figure 5). The buffering pH region (around pH 6) of the copolymers with histidine(Bzl) were distinctly broader compared with those without. This behavior was presumably attributed to the conjugated bonds of the imidazole groups, which allowed the imidazole groups to be protonated at acidic pH.[16] The mPEG-SS-Lys$_n$-r-His$_{20}$/nucleic acids complexes enabled escape from the endolysosome chambers and released into cytoplasm via the proton sponge effects. NaCl and PEI were used as control.

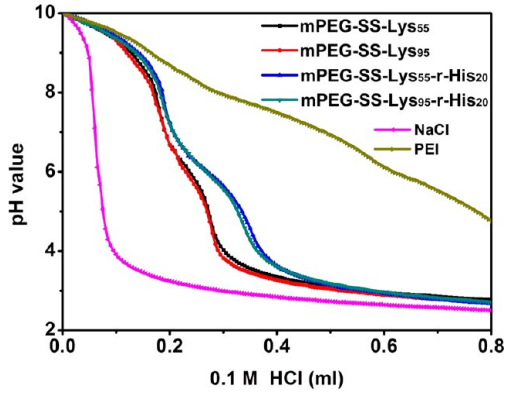

Figure 5. Buffering capacity of mPEG-SS-Lys$_n$-r-His$_m$ and PEI.

Agarose Gel Retardation Assay. The nucleic acids condensation and DNase protection ability of the copolymers were assessed by agarose gel retardation assay. As shown in Figure 6A–D, mPEG-SS-Lys$_{95}$/pDNA and mPEG-SS-Lys$_{95}$-r-His$_{20}$/pDNA complexes exhibit enhanced binding than mPEG-SS-Lys$_{55}$/pDNA and mPEG-SS-Lys$_{55}$-r-His$_{20}$/pDNA, which are completely condensed at weight ratios of 0.75 and 1, respectively. This is in agreement with the notion[17] that the DNA binding ability increases with charge density and the length of lysine. siRNA complexes were also evaluated (Figure 6E, F) at the same weight ratios as pDNA. It is found that the copolymers condensed siRNA preferably compared with pDNA under the same condition. Complete condensation weight ratios of mPEG-SS-Lys$_{55}$-r-His$_{20}$/siRNA and mPEG-SS-Lys$_{95}$-r-His$_{20}$/siRNA were found to be 0.75 and 0.5, respectively. These results indicate efficient encapsulation via hydrophobic histidylation at low molecular weight of siRNA.

DNase I protection ability of the complexes was also investigated considering that the complexes may suffer from endonucleases degrading upon reaching the tumor cells via intravenous administration. DNase I sufficiently acted on the mPEG-SS-Lys$_{55}$-r-His$_{20}$/pDNA and mPEG-SS-Lys$_{95}$-r-His$_{20}$/pDNA complexes (w/w = 1) at 37 °C for 10 min (Figure 6G, H). As no trace of the naked pDNA was observed, suggesting its complete degradation. In contrast, the pDNA encapsulated in mPEG-SS-Lys$_n$-r-His$_{20}$ demonstrated almost the same trace as the control in the wells. This result indicates adequate protection of pDNA by the mPEG-SS-Lys$_n$-r-His$_{20}$/pDNA complexes against DNase and other endonucleases.

Physiochemical Characteristics of mPEG-SS-Lys$_n$-r-His$_m$/pDNA Complexes. The size and ζ-potential of the mPEG-SS-Lys$_n$-r-His$_m$/pDNA complexes were investigated by dynamic light scattering (DLS). Morphometric observation of mPEG-SS-Lys$_{95}$-r-His$_{20}$ micelle was further studied by TEM. As shown in Figure 7A, the dynamic hydration diameter distribution of mPEG-SS-Lys$_{95}$-r-His$_{20}$ micelle is around 200 nm (PDI: 0.301). The inserted TEM image shows homogeneous spherical shape of the micelle with a diameter around 80 nm. The difference between the two results is associated with the shrinkage effect of the TEM sample. The mean particles size is kept below 200 nm (Figure 7C) and decreasing with the increasing weight ratios at the weight ratios >1:1. This is considered to be the suitable size range for efficient cellular uptake and circulation.[18]

The ζ-potential values of the mPEG-SS-Lys$_n$-r-His$_m$/pDNA complexes (Figure 7D) increased with the increasing weight ratios. To accelerate cellular uptake, positive charge is recommended for carriers to obtain preferable electrostatic interaction with the negatively charged cytomembranes. At the weight ratio > 2, the ζ-potentials of the four complexes were all positive and the highest value was under 30 mV, which was recognized to be within the optimum range of surface charge. Cytomembranes can be damaged by excess strong interaction with copolymers.[19]

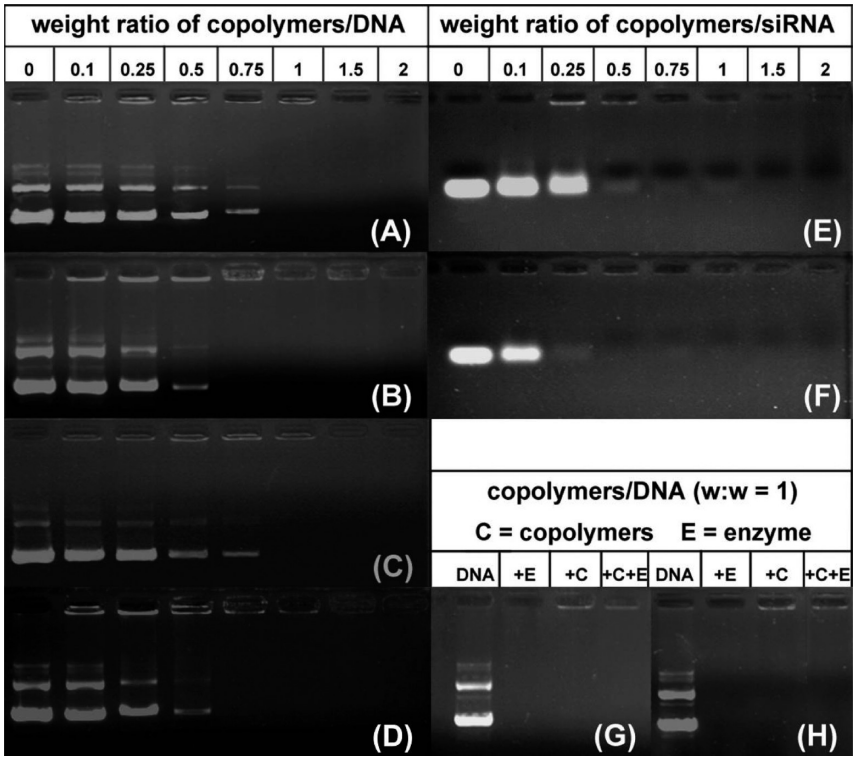

Figure 6. Agarose gel electrophoresis retardation assay of (A) mPEG-SS-Lys_{55}/pDNA, (B) mPEG-SS-Lys_{95}/pDNA, (C) mPEG-SS-Lys_{55}-r-His_{20}/pDNA, (D, G) mPEG-SS-Lys_{95}-r-His_{20}/pDNA, (E, H) mPEG-SS-Lys_{55}-r-His_{20}/siRNA, (F) mPEG-SS-Lys_{95}-r-His_{20}/siRNA complexes at weight ratios ranging from 0 to 2. The enzyme in panels G and H meant DNase I.

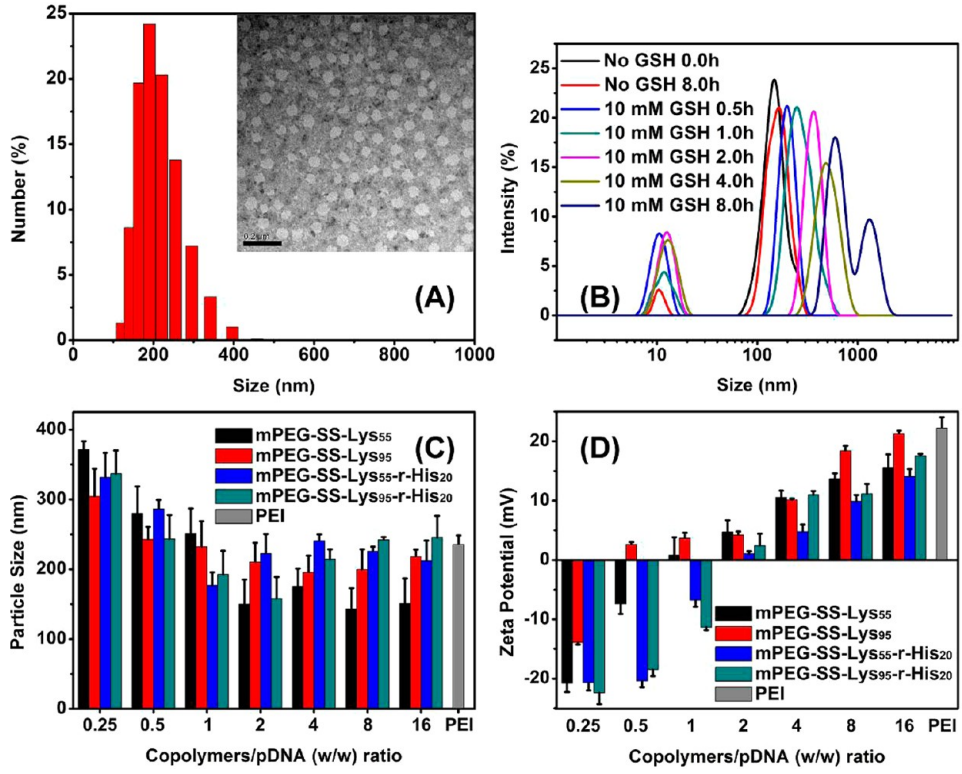

Figure 7. Size and ζ-potential distribution of mPEG-SS-Lys_n-r-His_m/pDNA. The dynamic hydration diameter distribution of mPEG-SS-Lys_{95}-r-His_{20} is shown in panel A with the inserted TEM image (bar: 0.2 μm). Size distribution results of mPEG-SS-Lys_{95}-r-His_{20}/pDNA complexes (w/w = 2) with 10 mM GSH are displayed in panel B. Mean particles size (C) and ζ-potential (D) of the mPEG-SS-Lys_n-r-His_m/pDNA complexes are measured at weight ratios from 0.25 to 16.

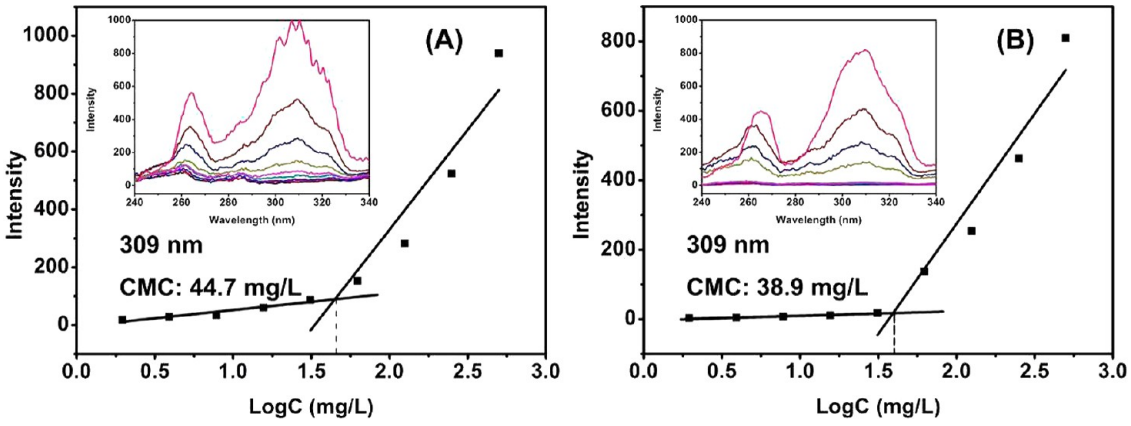

Figure 8. CMC fluorescence excitation spectra of pyrene with the inserted CMC curves of mPEG-SS-Lys$_{55}$-r-His$_{20}$ (A) and mPEG-SS-Lys$_{95}$-r-His$_{20}$ (B).

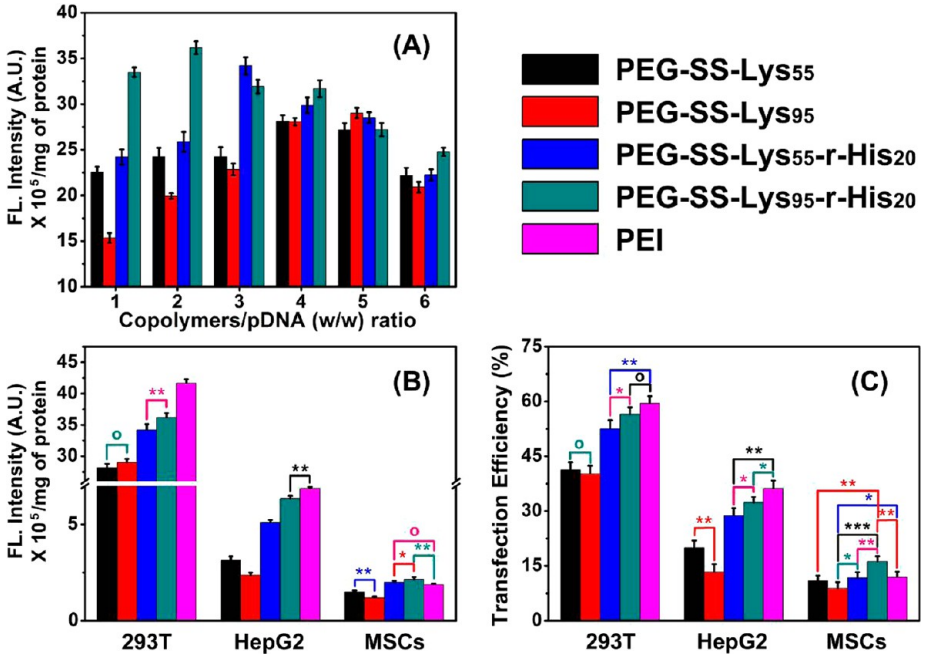

Figure 9. Quantitative transfection efficiency mPEG-SS-Lys$_n$-r-His$_m$/pEGFP complexes in 293T cells, HepG2 cells, and MSCs by BCA method and FCM. The fluorescence intensity per milligram of protein of the mPEG-SS-Lys$_n$-r-His$_m$/pEGFP complexes at weight ratios from 1 to 6 in 293T cells (A). (B) Fluorescence intensity per milligrams of protein and (C) FCM are the complexes at each optimum weight ratio in three kinds of cells. The results are presented as mean ± SD (n = 3). Statistical significance of the results are expressed as *$p \leq 0.05$, **$p \leq 0.01$, ***$p \leq 0.001$, $p > 0.05$. In B and C, each two data without marks means ***, except for MSCs in image C, which means ○.

For effectively releasing the gene encapsulated in the carriers into cytoplasm and decreasing cytotoxicity,[20] the gene carriers need to be disassembled and even degraded. Redox-sensitive disulfide bonds were introduced into the gene carrier for high intracellular GSH breaking of the disulfide bonds in order to remove the hydrophilic mPEG layer. The effects of GSH (10 mM) on the carriers were assessed by the particle size distribution for 8 h in PBS.

As shown in Figure 7B, particle sizes are rapidly increased over time in the presence of 10 mM GSH, and the mean size reaches 870.0 nm after 8 h. Some of the larger aggregates can be also observed by microscopy (see Figure S1 in Supporting Information). Meanwhile, the size change without GSH was negligible. The mPEG-SS-Lys$_{95}$-r-His$_{20}$/pDNA was found to be quite stable complexes. The sharply changed particle sizes were due to aggregation of cationic segments[6] via ionic interactions[21] after mPEG detachment. The hydrophilic mPEG shields were crucial to maintain stable complexes.

To demonstrate phase separation behavior, mPEG-SS-Lys$_n$-r-His$_m$ solution was subject to incubation with a hydrophobic probe pyrene, which is sensitive to hydrophobic microenvironment. Pyrene tends to accumulate in hydrophobic compartment with a usual fluorescence enhancement. Thus, pyrene was frequently employed to confirm micelles formation above the critical micelle concentration (CMC) characterized by fluorescence spectroscopy (Figure 8). The formation of the mPEG-SS-Lys$_n$-r-His$_{20}$ micelle structure was confirmed by CMC test and the results of mPEG-SS-Lys$_{55}$-r-His$_{20}$ and mPEG-SS-Lys$_{95}$-r-His$_{20}$ are 44.7 mg/L and 38.9 mg/L, respectively. CMC tests clearly indicate the phase separation of mPEG-SS-Lys$_n$-r-His$_m$ in aqueous solution.

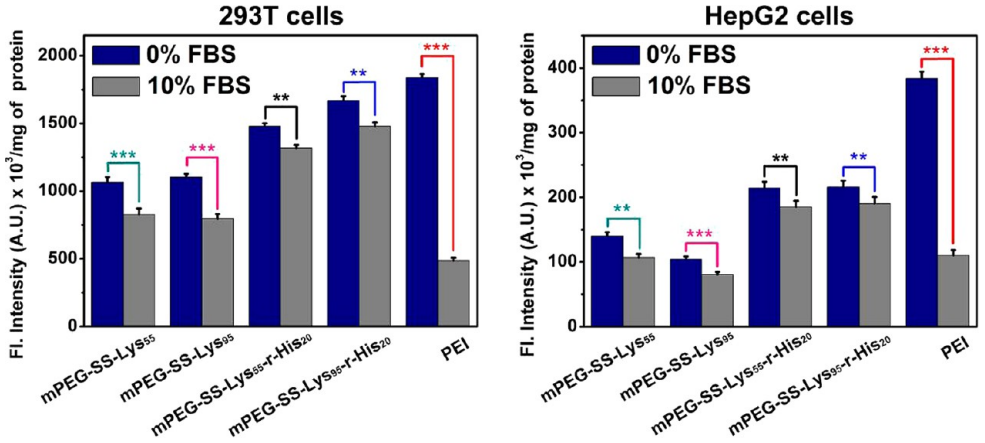

Figure 10. Transfection efficiency of mPEG-SS-Lys$_n$-r-His$_m$/pDNA complexes with or without 10% serum at each optimal weight ratio in 293T cells and HepG2 cells via BCA. The results are presented as mean ± SD (n = 3). Statistical significance of the results are expressed as $^{**}p \leq 0.01$, $^{***}p \leq 0.001$.

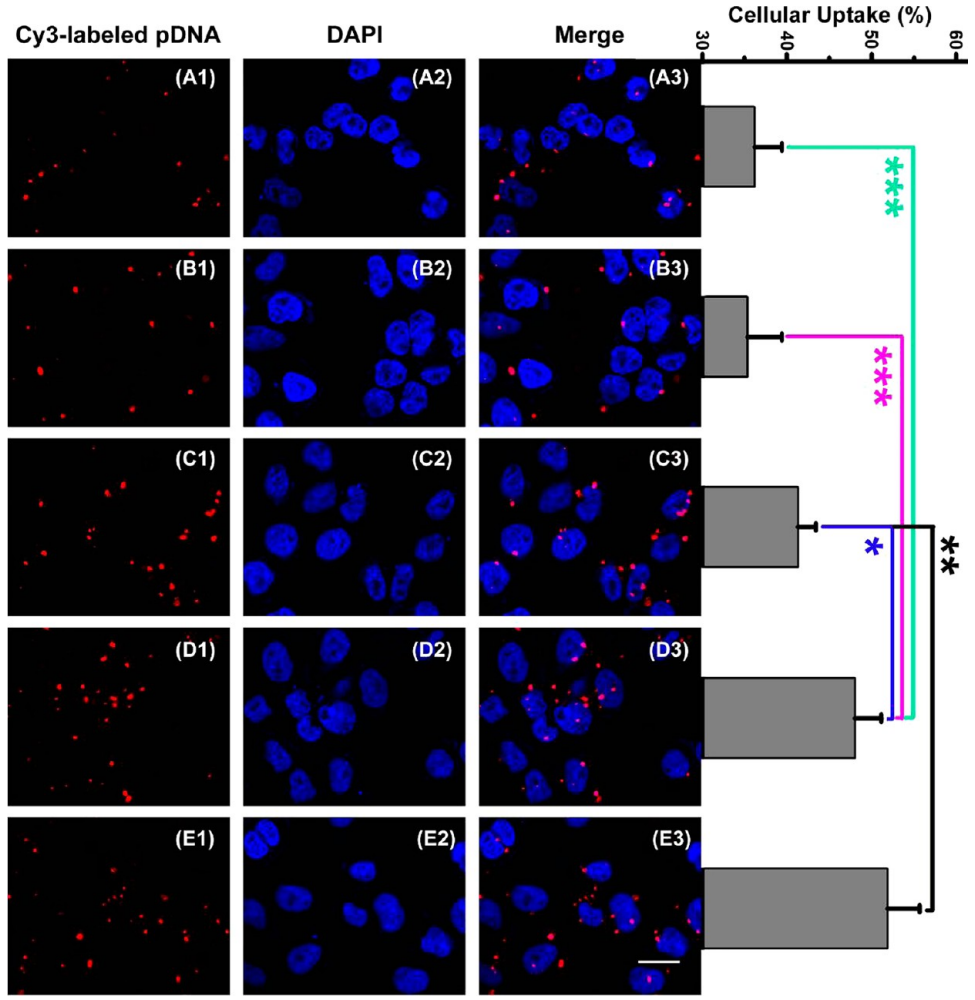

Figure 11. Cellular uptake by CLSM and FCM in HepG2 cells. CLSM images are Cy3-labeled pDNA (red), DAPI dyed nucleus (blue), and their merged pictures. Other images include mPEG-SS-Lys$_{55}$/pDNA (panel A, 4), mPEG-SS-Lys$_{95}$/pDNA (panel B, 5), mPEG-SS-Lys$_{55}$-r-His$_{20}$/pDNA (panel C, 3), mPEG-SS-Lys$_{95}$-r-His$_{20}$/pDNA (panel D, 2), PEI/pDNA (panel E, 1.3). The FCM results are presented as mean ± SD (n = 3). Statistical significance of the results are expressed as $^{*}p \leq 0.05$, $^{**}p \leq 0.01$, $^{***}p \leq 0.001$. Bar: 25 μm.

In Vitro Transfection Efficiency of mPEG-SS-Lys$_n$-r-His$_m$/pEGFP Complexes. To assess the in vitro transfection efficiency of the mPEG-SS-Lys$_n$-r-His$_m$ gene vectors, 293T cells, HepG2 cells, and MSCs were selected as model cells and tested by the BCA method and FCM. PEI was employed as a positive control. The reporter plasmid pEGFP was complexed with PEI at weight ratios of 1.3 or mPEG-SS-Lys$_n$-r-His$_m$ from 1 to 6, at which all four copolymers had complete binding ability.

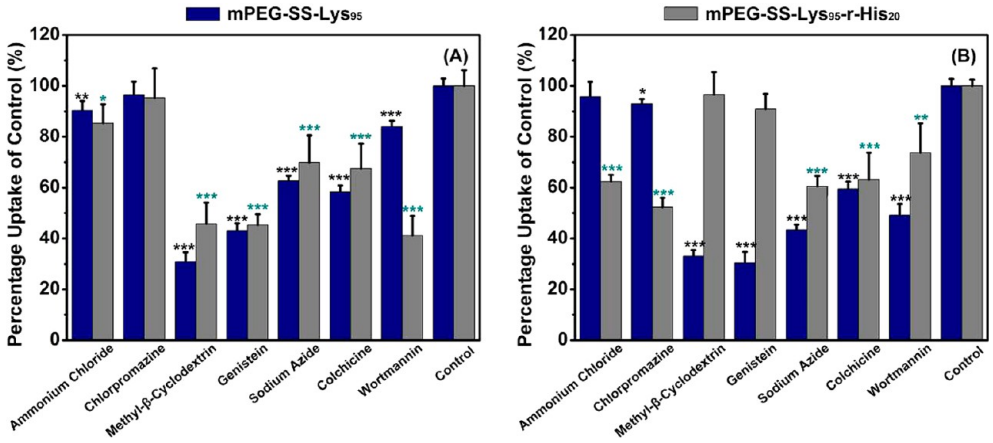

Figure 12. Cellular uptake percent of FITC-mPEG-SS-Lys_{95} and FITC-mPEG-SS-Lys_{95}-r-His_{20} in 293T cells (A) and HepG2 cells (B) following 0.5 h preincubation and 4 h coincubation with different inhibitors. The results are presented as mean ± SD (n = 5). Statistical significance of the results compared with the control are expressed as $^{*}p \leq 0.05$, $^{**}p \leq 0.01$, $^{***}p \leq 0.001$.

Figure 9A shows the fluorescence intensity per milligram of protein in 293T cells at weight ratios from 1 to 6. From this quantitative assay, the optimal weight ratios of each copolymer/pEGFP for transfection were determined and used in the subsequent experiments. The optimal weight ratios of mPEG-SS-Lys_{55}/pEGFP, mPEG-SS-Lys_{95}/pEGFP, mPEG-SS-Lys_{55}-r-His_{20}/pEGFP, and mPEG-SS-Lys_{95}-r-His_{20}/pEGFP were 4, 5, 3, and 2, respectively. As shown in Figure 9A, the transfection efficiency exhibits a decrease at a given weight ratio for different copolymers. This is associated with the excess positive charges from the copolymers resulting from hyper-compact interactions and difficulty in pEGFP release.[22] The same results were found in HepG2 cells and MSCs for the identical experiments (Supporting Information Figure S2).

Figure 9B, C shows the quantitative assays of the five complexes at each optimal weight ratios in three cells by BCA and FCM, respectively. In 293T and HepG2 cells, PEI exhibits the best transfection efficiency (4165 ± 65, 687 ± 8 au × 10^3/mg of protein for BCA method, 59.46 ± 1.99%, 36.16 ± 2.19% for FCM). There is no significant difference between mPEG-SS-Lys_{95}-r-His_{20} (56.46 ± 1.89% for FCM) and PEI in 293T cells ($p > 0.05$). The histidylation of polylysine is considered to improve the transfection efficiency for its proton sponge effect, which is in line with the previous report.[23]

It is to be noticed that the transfection efficiency of mPEG-SS-Lys_{95}-r-His_{20} in MSCs was significantly higher than that of PEI ($p < 0.01$) both in fluorescence intensity (215 ± 11, 187 ± 5 au × 10^3/mg of protein) and cells numbers (16.18 ± 1.43%, 11.88 ± 1.52%). The statistical significance in MSCs was possibly due to the components of the mPEG-SS-Lys_{95}-r-His_{20} with favorable biocompatibility and low toxicity, providing better conditions for MSCs.

Figure 9B and C shows less transfection efficiency of mPEG-SS-Lys_n than mPEG-SS-Lys_n-r-His_{20} in all three different cells. It is attributable to the proton sponge effect provided by the imidazole ring of the histidine(Bzl). For a given length of His segment, mPEG-SS-Lys_{95}-r-His_{20} exhibits better transfection efficiency compared to mPEG-SS-Lys_{55}-r-His_{20}. The qualitative fluorescence and bright field images of mPEG-SS-Lys_n-r-His_m/pEGFP complexes and PEI/pEGFP at each optimal weight ratio are presented in Supporting Information Figure S3. The green cells suggest successful delivery of copolymers/pEGFP, and the density of the fluorescent cells is proportional to the transfection efficiency.

For imitating of the physiological environment, an assay of transfecting the cells with 10% serum was carried out and measured by BCA. As shown in Figure 10, cells of gene expression transfected by PEI/pDNA complexes with 10% serum are dramatically reduced by 3.8 and 3.5 fold compared with that without serum in 293T cells and HepG2 cells, respectively, while mPEG-SS-Lys_n-r-His_m/pDNA transfected cells show minor decrease in 293T cells and HepG2 cells, respectively. The results suggest that the PEI/pDNA complex effectively maintains its high transfection efficiency with 10% serum for high density positive charges.[24] Hence, PEI was not recommended to be applied in vivo. It should be noted that mPEG-SS-Lys_n-r-His_{20}/pDNA complexes (10 percentages decrease) showed the highest resistant capability for serum.

Cellular Uptake and Intracellular Distribution of the mPEG-SS-Lys_n-r-His_m/pDNA Complexes. To examine the feasibility of the mPEG-SS-Lys_n-r-His_m/pDNA complexes for cellular entry, which was the prerequisite condition of the downstream gene expression, CLSM and FCM assays were conducted for cellular uptake. HepG2 cells were incubated with four mPEG-SS-Lys_n-r-His_m/pDNA (Cy3-labeled) complexes for 4 h and then prepared for CLSM and FCM. PEI/pDNA complex was served as positive control. As shown in Figure 11, most pDNA is located in the perinuclear region by mPEG-SS-Lys_n/pDNA complexes incubated, and a great deal of pDNA have entered nuclear by mPEG-SS-Lys_n-r-His_{20}/pDNA complexes incubated. The images confirmed that the mPEG-SS-Lys_n-r-His_m/pDNA complexes successfully delivered pDNA into the nuclear. The statistical significance of the cellular uptake results by FCM was calculated. Except for mPEG-SS-Lys_{95}-r-His_{20} (48.09% ± 3.1) and PEI (51.92% ± 3.8) having no difference in cellular uptake, there were significant difference between the other three copolymers and PEI.

Cellular uptake pathway of the copolymers was explored by coincubation with clathrin-mediated endocytosis inhibitors (ammonium chloride[25] and chlorpromazine), caveolae-mediated endocytosis inhibitors (M-β-CD and genistein), macropinocytosis inhibitior (wormannin),[26] as well as the ATP synthesis inhibitor (sodium azide) and actin polymerization inhibitor (colchicine).[27] The concentrations of all inhibitors are adjusted to ensure no effect on cell viability. As shown in Figure

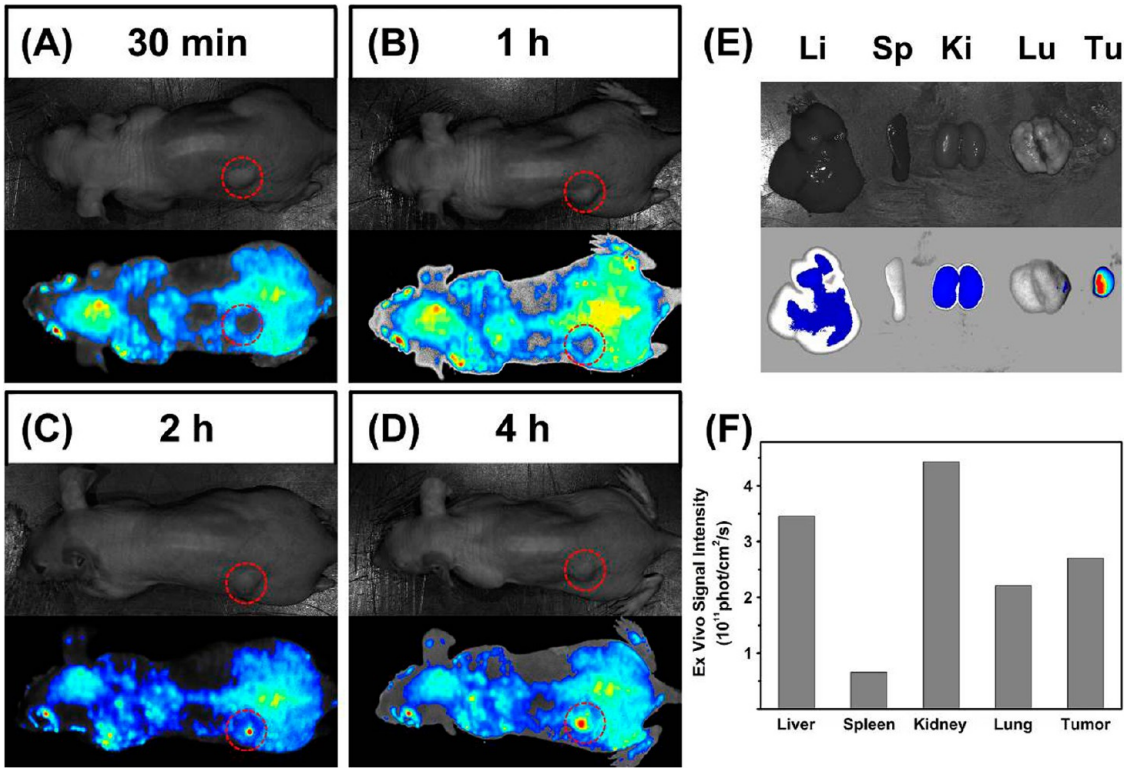

Figure 13. In vivo distribution of BODIY-mPEG-SS-Lys$_{95}$-r-His$_{20}$ at different time (A–D) after intravenous administration in a mice-bearing HepG2 tumor. Liver, spleen, kidney, lung, and tumor are excised, imaged (E), and quantitative analyzed (F) in 4 h after injection.

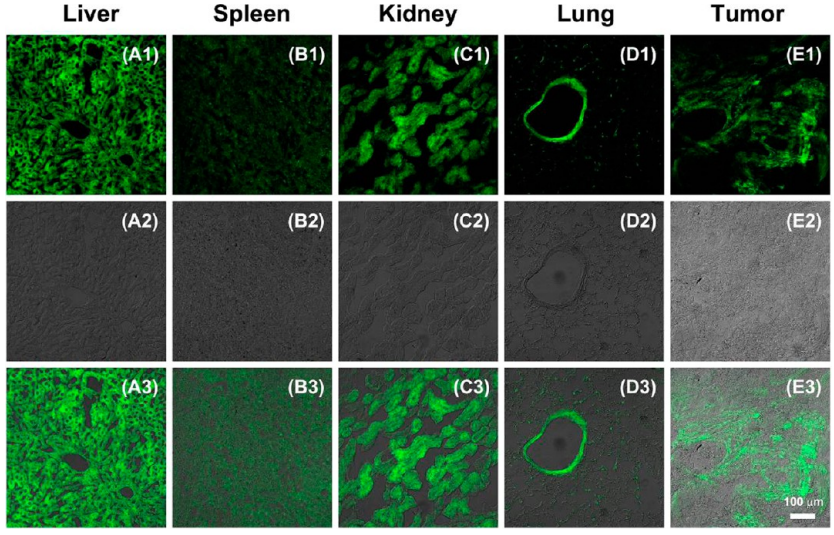

Figure 14. In vivo transfection results of mPEG-SS-Lys$_{95}$-r-His$_{20}$/pEGFP complexes (w/w = 2) at 7 days after intravenous administration in HepG2 tumor-bearing mouse. Bar: 100 μm. Panel 1: fluorescence field. Panel 2: bright field. Panel 3: merge.

12, mPEG-SS-Lys$_{95}$ has entered cells via caveolae-mediated endocytosis and macropinocytosis in both 293T and HepG2 cells. However, mPEG-SS-Lys$_{95}$-r-His$_{20}$ shows different entry behavior into 293T cells via caveolae-mediated endocytosis and macropinocytosis, while it was internalized into HepG2 cells via clathrin-mediated endocytosis and macropinocytosis. The cytotoxicity of FITC-mPEG-SS-Lys$_n$-r-His$_m$ was considered ineffective to this experiment (Supporting Information Figure S4).

In view of the above, mPEG-SS-Lys$_{95}$-r-His$_{20}$ was supposed to be transported to endolysosome for its clathrin-mediated endocytosis in HepG2 cells. The experimental results indicate that it exhibits the best transfection efficiency in four different mPEG-SS-Lys$_n$-r-His$_m$ carriers, due to hydrophobic histidylation.[28] With respect to macropinocytosis in both entry pathways of the vectors, the cells are able to phagocytize particles below 200 nm.

The cells treated with sodium azide can phagocytize FITC-mPEG-SS-Lys$_n$-r-His$_m$ rather than complete inhibition. This behavior suggests that glucose and exogenous ATP in the cultural medium supplies energy for the phagocytosis process.[27] Colchicine is able to block actin polymerization, that is required

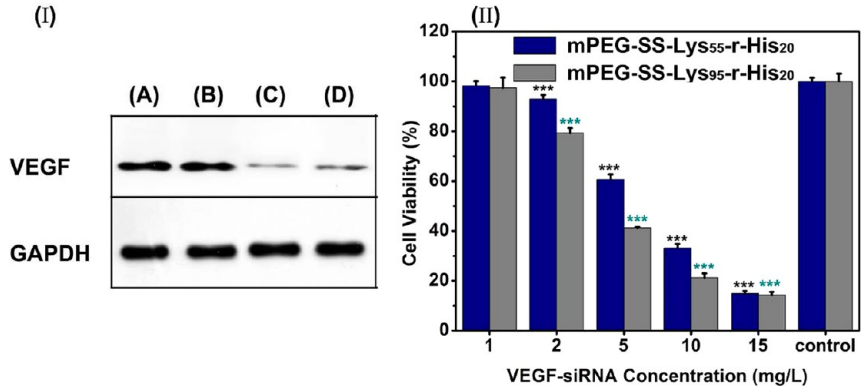

Figure 15. Western blot analysis (I) and cell viability (II) in HepG2 cells in vitro. The cells are transfected with mPEG-SS-Lys$_n$-r-His$_{20}$/VEGF-siRNA at each optimal weight ratio with changed VEGF-siRNA amounts for 48 h. 10 mg/L VEGF-siRNA group is used for Western blot. (A) Blank control, (B) PEI/NC-siRNA, (C) mPEG-SS-Lys$_{95}$-r-His$_{20}$/VEGF-siRNA, and (D) mPEG-SS-Lys$_{55}$-r-His$_{20}$/VEGF-siRNA. The results are presented as mean ± SD (n = 3). Statistical significance of the results compared with the control are expressed as $^{***}p \leq 0.001$.

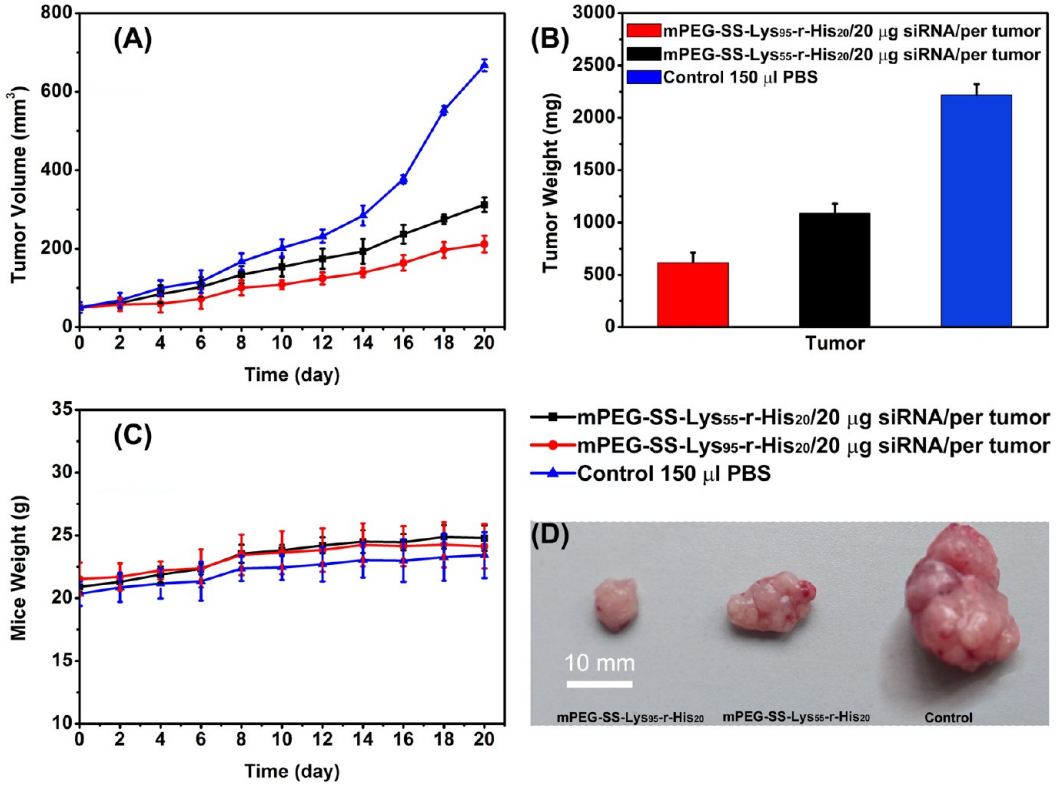

Figure 16. In vivo antitumor application of mPEG-SS-Lys$_n$-r-His$_{20}$/VEGF-siRNA intravenous administrated at each optimal weight ratio in mice-bearing subcutaneous HepG2 tumor. PBS serves as control. (A) tumor volume, (B) tumor weight, (C) mice weight, and (D) representative tumor photograph. The results are presented as mean ± SD (n = 5).

for clathrin- and caveolae- mediated endocytosis.[29] As a result, it causes the decrease of FITC-mPEG-SS-Lys$_n$-r-His$_m$ entry, suggesting at least one endocytosis is involved in the cellular uptake pathway.

Biodistribution of mPEG-SS-Lys$_{95}$-r-His$_{20}$ in Mice Bearing HepG2 Tumor. For effective in vivo application, it was necessary to investigate the biodistribution of gene complexes, which should mainly aggregate in the tumor site rather than other visceral organs. The mouse bearing HepG2 tumor was imaged from 30 min to 4 h after intravenously injected with BODIPY-mPEG-SS-Lys$_{95}$-r-His$_{20}$.

From Figure 13A–D, the vector gradually aggregates in the subcutaneous tumor from the border over time. Based on the theory of enhanced permeability and retention (EPR) effects, this is caused by the local leaky vasculature in tumor sites[30] and leading to effective accumulation of particles size around 150 nm on tumor sites.[27] A longer time observation (24 h) has been shown in the Supporting Information Figure S5. It can be found considerable accumulation in both liver and tumor but with a reduced fluorescent intensity in kidney in comparison with the short time groups.

The fluorescence intensity of the labeled vector in the main organs is qualitatively and quantitatively shown in Figure 13E and F. It was found that the vector distributed primarily in the liver and kidney, due to the nonspecific arrest by the mononuclear phagocyte system (MPS).[31] The distribution of

the vector in tumor-bearing mouse indicates the feasibility of the subsequent exogenous gene expression in vivo. Results of the mouse treated with PBS are not shown, as no GFP fluorescence was found.

In Vivo Gene Expression of mPEG-SS-Lys$_{95}$-r-His$_{20}$/pEGFP in Mice Bearing HepG2 Tumor. After the observation of mPEG-SS-Lys$_{95}$-r-His$_{20}$ distribution, 7-day in vivo transfection ability of the mPEG-SS-Lys$_{95}$-r-His$_{20}$ was investigated to further confirm the effective gene expression in the tumor and retention in other viscera organs. The results are shown as CLSM images, which are photographed under the same exposure conditions (Figure 14). The fluorescence intensity of GFP in liver and kidney is noticeably stronger than that in spleen and lung, which is consistent with biodistribution.

Most of the tumor cells also expressed GFP suggesting that mPEG-SS-Lys$_{95}$-r-His$_{20}$ was a promising gene vector for bioapplication. A sufficient long circulation of mPEG-SS-Lys$_{95}$-r-His$_{20}$ in the bloodstream was found during effective gene expression in vivo. The vector coated with mPEG shells successfully circulated in vasculature rather than aggregated and precipitated with negatively charged serum protein in vasculature. The spleen and lung that also expressed a small amount GFP was attributed to the long circulation and the reticuloendothelial system (RES).

Antitumor Effect of mPEG-SS-Lys$_n$-r-His$_{20}$/VEGF-siRNA Complexes. The mPEG-SS-Lys$_n$-r-His$_{20}$ gene vectors were designed not only for pDNA but also for siRNA, which was recommended to be complexed with mPEG-SS-Lys$_n$-r-His$_{20}$ as transfection reagents for gaining better complex stability than conventional cationic polymers.[5]

Successful complexation and compaction behaviors between mPEG-SS-Lys$_n$-r-His$_{20}$ and VEGF-siRNA are shown in Figure 6E and F. The antitumor effect in cellular level was detected by MTT assay and Western blot. As shown in Figure 15II, when the VEGF-siRNA concentration of mPEG-SS-Lys$_n$-r-His$_{20}$/VEGF-siRNA complexes is higher than 2 mg/L, both complexes exhibit significant cell viability inhibition. The Western blot result (Figure 15I) verified the pronounced gene transfection in the protein level. In agreement with MTT assay, mPEG-SS-Lys$_{95}$-r-His$_{20}$ possessed preferable growth suppression compared with mPEG-SS-Lys$_{55}$-r-His$_{20}$ (siRNA concentration: 10 mg/L). Figure 15A and B show blank control and PEI/NC-siRNA as negative control, respectively.

In vivo experiment was carried out by mPEG-SS-Lys$_n$-r-His$_{20}$. Subcutaneous HepG2 tumor model was established in BALB/c nude mice. When the tumor volume reached approximately 50 mm^3, intravenous administration of the mPEG-SS-Lys$_n$-r-His$_{20}$/VEGF-siRNA complexes (20 μg VEGF-siRNA/per mouse, once every 2 days, 10 times) and PBS began. The initial tumor volume (50 mm^3) was chosen referring to the previous reports,[32,33] suggesting the VEGF protein in relative low expression.

As indicated in Figure 16A, the mPEG-SS-Lys$_{95}$-r-His$_{20}$/VEGF-siRNA group shows the most significant growth inhibition. mPEG-SS-Lys$_{55}$-r-His$_{20}$/VEGF-siRNA group comes to the second (volume on day 22:211 ± 21 mm^3, 312 ± 19 mm^3). In sharp contrast, the volume of the PBS group at the same stage increases to 667 ± 15 mm^3 with the weight of 2216 ± 105 mg. The tumor weights for mPEG-SS-Lys$_{95}$-r-His$_{20}$ and mPEG-SS-Lys$_{55}$-r-His$_{20}$ (Figure 16B) after dissecting at day 22 are 616 ± 97 mg and 1090 ± 90 mg, respectively. The tumor volume and weight shows promising tumor suppressive effect. A representative tumor photograph for qualitative results is shown in Figure 16D, except for the pronounced size difference of the tumors. It is worth noting that the color of the fresh tumors exhibits distinct difference. The PBS group tumor is red with abundant blood microvessels on the surface, while the mPEG-SS-Lys$_{95}$-r-His$_{20}$/VEGF-siRNA group tumor is pink with fewer blood microvessels. The results are attributed to effective VEGF inhibition.

The mice weight (Figure 16C) slowly increases and shows no difference among the three groups during the entire experiment, suggesting no toxic effects on mice. All mice survived until the end point of experiments. The tumors in Figure 16D are also accepted Western blot analysis (Figure 17).

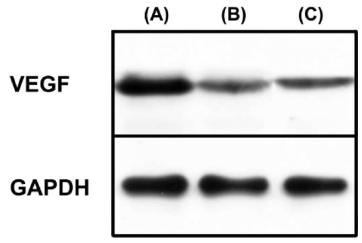

Figure 17. Western blot analysis of the tumor in Figure 15C. (A) PBS, (B) mPEG-SS-Lys$_{95}$-r-His$_{20}$/VEGF-siRNA, (C) mPEG-SS-Lys$_{55}$-r-His$_{20}$/VEGF-siRNA.

Brightness difference of the bands between treated and control group decreases in tissue compared with that in cellular level. This circumstance sets a good example for varying levels of bioavailability in gene transfection,[34] in vitro and in vivo. The underlying mechanism for this behavior requires further investigation. The efficient systemic delivery ability of mPEG-SS-Lys$_n$-r-His$_{20}$/nucleic acids complexes can successfully deliver nucleic acids into tumor cells and provide a feasible strategy for systematic tumor gene therapy.

CONCLUSIONS

In this study, we have successfully developed a dual functionalized gene vector for both pDNA and siRNA transfection in vitro and in vivo. Hydrophobic histidylation facilitates the formation of stable complexes. Histidine segment provides proton buffering capacity to improve the gene transfection efficiency. Cleavable mPEGylation has been introduced to prolong the systemic circulation, while allowing for selective PEG detachment under tumor relevant reduction condition. This process has been shown to have effect on the subsequent gene releasing into cytoplasm. The experimental results have shown high transfection efficiency of the mPEG-SS-Lys$_n$-r-His$_m$ gene vector in vivo. Therefore, mPEG-SS-Lys$_n$-r-His$_m$ will provide a clinically viable vector for nonvirus gene delivery.

EXPERIMENTAL SECTION

Materials. Monomethyl ether poly(ethylene glycol) carboxymethyl (mPEG-COOH, MW = 2000 g/mol) was obtained from Yare Biotech(China), and ε-benzyloxycarbonyl-L-lysine was purchased from GL Biochem (China). 1-Benzyl-N-carbobenzoxy-L-histidine (His(Bzl)-Cbz), triethylamine (Et_3N, 99%), cystamine dihydrochloride (98%), branched polyethyeneimine (MW = 25000, bPEI$_{25k}$, PEI) and GSH were obtained from Sigma-Aldrich (Natick, MA). Tetrahydrofuran (THF, 99.85%), 1,4-dioxane (99.8%), dimethylformamide (DMF), and hydrogen bromide (HBr) 33 wt % solution in glacial acetic acid were purchased from Acros Organics. Triphosgene (99%), dichloro-

methane (DCM), thionyl chloride ($SOCl_2$), *n*-hexane, dimethyl sulfoxide (DMSO) were supplied from Aladdin and used as received. Dulbecco's modified Eagle's medium (DMEM), fetal bovine serum (FBS), 1% penicillin−streptomycin (PS), 0.25% trypsin−EDTA, phosphate buffered saline (PBS) and BODIPY 650/665-X were purchased from Gibco Invitrogen. Deoxyribonuclease I (DNase I), 3-(4,5-dimethylthiazol-2-yl)-2,5-dipenyltetrazoium bromide (MTT) and bicinchoninic acid (BCA) protein assay kit were purchased from Beyotime Institute of Biotechnology (China). Label IT-TrackerCy3 Kit was obtained from Mirus Bio LLC. The reporter gene plasmid, pEGFP-C1 was supplied from Invitrogen.

Synthesis of mPEG-SS-NH_2. To activate mPEG-COOH, N,*N*′-dicyclohexylcarbodiimide (DCC, 0.25 g, 1.2 mmol), *N*-hydroxy succinimide (NHS, 0.14 g, 1.2 mmol) were mixed with mPEG-COOH (2 g, 1 mmol) in anhydrous DCM (40 mL) at 0 °C for 5 h. Then, under a nitrogen atmosphere, dry cystamine (1 g, 7 mmol) in 10 mL DCM was dropwise added in the above mixture and kept stirring at RT for 24 h. The reaction production was filtrated, washed twice with cold diethyl ether and dialyzed with a membrane (MWCO 1000 Da) for 48 h. The purified yield of mPEG-SS-NH_2 was 80%, which was calculated after lyophilization.

Synthesis of ε-Benzyloxycarbonyl-L-lysine N-Carboxyanhydride (Lys(Cbz) -NCA) and 1-Benzyl-L-histidine N-Carboxyanhydride (His(Bzl)-NCA). Dry Lys(Cbz) (11.2 g, 40 mmol) and triphogene (5 g, 16.8 mol) were dissolved in anhydrous THF, respectively. The triphogene was slowly dropwise added into Lys(Cbz) and the reaction was performed at 50 °C in an oil bath with N_2 protection. When the solution was clear, the reaction was accomplished. Then, the crude product was poured into excess dry *n*-hexane to elevate crystallization of the Lys(Cbz)-NCA at −20 °C overnight. The crude material was further recrystallized twice from anhydrous THF/*n*-hexane (1:15, v/v). At last, the resulting product was dried under vacuum at 30 °C for 24 h and the purified yield was 90%.

The procedures of His(Bzl)-NCA synthesis was adapted from the literature.[35] $SOCl_2$ (2 mL) was dropwise added into the mixture of His(Bzl)-Cbz (2 g, 5.3 mmol) and anhydrous 1,4-dioxane (10 mL). The reaction was performed under stirring at room temperature for 3 h with N_2 protection. The NCA was precipitated by diethyl ether to form His(Bzl)-NCA·HCl crystals and dried under vacuum. Et_3N (1 mL) and the His(Bzl)-NCA·HCl (∼2 g) were mixed in DMF (10 mL) to form trithylammonium hydrochloride and were filtrated to remove hydrochloride. The filtrate was dialyzed and freeze-dried. The yield was 70%.

Synthesis of mPEG-SS-Lys_n-r-His_m Random Copolymers and mPEG-SS-Lys_n Copolymers. The copolymers were prepared by the ring-opening polymerization of the Lys(Cbz)-NCA and His(Bzl)-NCA and the amino group of mPEG-SS-NH_2 as initiator.[36] The reactions between various feed ratios of the three monomers in DMF were conducted at RT under nitrogen for 3 days. The products were dialyzed against water for 3 days, followed by frozen-drying.

The benzyloxycarbonyl group of the products was removed according to the protocol in our laboratory.[7] Briefly, 800 mg copolymer was dissolved in TFA (8 mL) and was stirring at 0 °C under N_2. Then, HBr 33 wt % solution in glacial acetic acid (4 mL) was added in an equal amount every hour. The products were rotary steamed at 55 °C, dissolved in DMF and dialyzed with a dialysis membrane (MWCO 3500 Da) for 3 days. The resulting production was filtrated by a 450 nm membrane and frozen-dried. The purified yields of mPEG-SS-Lys_{55}, mPEG-SS-Lys_{95}, mPEG-SS-Lys_{55}-r-His_{20}, and mPEG-SS-Lys_{95}-r-His_{20} were 65%, 66%, 71%, and 69%, respectively. The letter r means random.

Characterization. ^1H NMR spectra were obtained using a NMR spectrometer (Switzerland, Avance500 MHz) in D_2O or DMSO-d6, TMS as standard. The morphology of the mPEG-SS-Lys_{95}-r-His_{20} copolymer was observed by H7100 TEM at an acceleration voltage of 100 kV after negatively stained by phosphotungstic acid (0.01 w/v %, 10 μL, 20 s). The TEM sample was prepared as the previous report.[37] The critical micelle concentration (CMC) measurement was conducted referring to the published article.[38] The intensities at 309 nm were considered as a function of the polymer concentrations according to the pyrene excitation spectra. Both excitation and emission bandwidth were 4 nm.

Buffering Capacity. The buffering capacity of the copolymers was measured by acid−base titration.[6] In brief, copolymers (6 mg) were dissolved in 150 mM NaCl (30 mL) and were adjusted to pH 10 with 0.1 M NaOH. The solutions were stepwise added 0.1 M HCl (5 μL each time), and the pH values measured by a microprocessor pH meter were recorded.

Preparation of mPEG-SS-Lys_n-r-His_m/Nucleic Acids Complexes. Before mixing with nucleic acids, the mPEG-SS-Lys_n-r-His_{20} was freshly prepared by being dissolved in DMF, dialyzed against distilled water and frozen-dried. Then, mPEG-SS-Lys_n-r-His_{20} and mPEG-SS-Lys_n were dissolved in 150 mM NaCl, respectively, and were mixed with pEGFP-C1 to form complexes at various weight ratios. The complexes were gently vortexed for 10 s and incubated at 37 °C for 30 min before use.

Agarose Gel Retardation Assay and DNase I Protection Assay. To evaluate the DNA condensation ability of mPEG-SS-Lys_n-r-His_m copolymers, we prepared the nucleic acids complexes at weight ratios ranging from 0.1 to 2 as the aforementioned method. Then, the complexes (10 μL) containing 0.5 μg pDNA or siRNA were electrophoresed onto 1% (w/v) agarose gel with ethidium bromide. The electrophoresis was run in TAE buffer at 100 V for 40 min (pDNA) or 15 min (siRNA). The nucleic acids bands were visualized by a UV lamp using a GelDoc system (Imago).

The DNase I protection assay was analogous to the above assay with some modification.[39] In brief, before being loaded on the agarose gel, the pDNA complexes were incubated with DNase I at 37 °C for 10 min and terminated by 25 mM EDTA (1 μL) at 65 °C for 10 min.

Particle Size and ζ-Potential Measurement. The particle size and ζ-potential of pDNA complexes were characterized by a Nano-ZS 90 Nanosizer (Malvern Instruments, Worcestershire, U.K.). The pDNA complexes at weight ratios from 0.25 to 16 were fabricated according to the foregoing method and diluted with 1 mL 150 mM NaCl before being measured. PEI/pDNA (w/w = 1.3) complexes served as control. The effect of GSH on the stability of mPEG-SS-Lys_{95}-r-His_{20}/pDNA complexes was assessed by observing the size change of the complexes at different time points[7] by DLS and microscope. GSH was added into the solutions to form the 10 mM GSH final concentration.

Cell Culture and Animal Models. Human embryonic kidney transformed 293 (293T) cells and human hepatocellular carcinoma (HepG2) cells were purchased from the Cell Center of the Tumor Hospital of Fudan University. Rat bone mesenchymal stem cells (MSCs) were kindly provided by the Stem Cell Center of Tongji University. The cells were cultured in full medium (89% high/low-glucose DMEM, 10% FBS and 1% PS) at 37 °C under a 5% CO_2 humidified atmosphere. When the confluence reached 90%, the cells were harvested by 0.25% trypsin-EDTA and centrifugation. Then, the cell suspensions were used for the following cell tests.

7 ×10^6 freshly harvested HepG2 cells in 100 μL PBS were inoculated subcutaneously into the left posterior limb of the BALB/c nude mouse (4−5 weeks, male, Shanghai SLC, China). The nude mice could be used for in vivo tests, when the tumor volume would reach 50 mm^3. All the animal experimental protocols were in strict accordance with protocols approved by the guidelines of Animal Care and Use Committee of Tongji University.

Cytotoxicity Assay. The cytotoxicity assay of the copolymers was assessed by the MTT method[14] with 293T cells, HepG2 cells and MSCs. Briefly, 5 × 10^3 cells were seeded in a 96-well plate in 100 μL full medium. Next day, the cells were exposed to gradient concentrations of the copolymers ranging from 11 to 200 mg/L in 200 μL fresh pure DMEM for another 24 h. Then 20 μL MTT (5 mg/mL) and 150 μL DMSO were procedurally added. Each sample had five parallel wells. The Multiscan MK3 microplate reader (Thermo Fisher Scientific, Waltham, MA, U.S.A.) was used to measure the optical density (OD) at 570 nm. The relative cell viability was calculated by the following equation: the viability (%) = (ODsample/ODcontrol) × 100.

In Vitro Transfection. 293T cells, HepG2 cells, and MSCs were used to performed the in vitro transfection evaluated by BCA protein assay kit[40] and flow cytometry method (FCM). The reporter plasmid, pEGFP, was used for the qualitative and quantitative determination. PEI was used for positive control at weight ratio of 1.3.[41] Briefly, 293T cells (8×10^4 cells/well), HepG2 cells (6×10^4 cells/well) and MSCs (5×10^4 cells/well) were seeded into 24-well plate in full medium, respectively. After 24 h, the copolymers/pDNA complexes (0.5 μg pDNA per well) were prepared at weight ratios from 1 to 6 in pure DMEM and added in each well containing 400 μL fresh pure DMEM. After 4 h, the mixed medium was substituted for full medium and the cells were incubated for additional 44 h before the determination.

To evaluate the serum effect on transfection at a cellular level, 10% FBS was added into the DMEM in the 4 h-incubation. All the samples conducted three dependent tests. For qualitative observation, the transfected cells were imaged under an inverted fluorescence microscope (Nikon Ti−S invert, ECLIPSE 80i).

For the GFP relative quantitative determination, cells were washed by PBS and cracked by reporter lysis buffer (200 μL, Promega, U.S.A.). Then 100 μL lysates were used for determining the fluorescence intensity by a fluorospectro photometer (Fluoroskan Ascent FL, Thermo Scientific) at excitation 488 nm and emission 509 nm. The rest was used for analyzing the total protein content by BCA protein assay kit according to the manufacturer's instruction.

For the GFP quantitative determination, the cells were prepared in infixative (PBS with 2% paraformaldehyde) and measured by a flow cytometer (FACScan, Becton, and Dichinson). The transfection efficiency was described as the percentage of the GFP-positive cells.

Cellular Uptake. The pDNA used in the cellular uptake assays was labeled by Cy3 with the method recommended by manufacturer. The cellular uptake behavior was assessed by confocal laser scanning microscopy (CLSM, Leica TCS SP5 II) and FCM. HepG2 cells (2×10^5 cells/well) were seeded into 6-well plate using coverslip culture method for 24 h before transfection. The copolymers/Cy3-labeled pDNA complexes at each optimal transfection weight ratio were incubated with the cells for 4 h in pure DMEM. For the CLSM assay, the cells were treated with PBS washing, 4% paraformaldehyde fixing, DAPI dying, and glycerin sealing.

Cellular Uptake Pathway. 293T cells and HepG2 cells were preincubated with various inhibitors in pure DMEM (200 μL) for 30 min in 96-well plate,[42,43] followed by adding 5 μg FITC-mPEG-SS-Lys_{95}-r-His_m and incubating for another 4 h. The following inhibitors were used, sodium azide (10 mM),[27] colchicine (40 μg/mL),[43] chlorpromazine (10 μg/mL),[42] NH_4Cl (50 mM),[42] methyl-β-cyclodextrin (M-β-CD, 10 mM),[42] genistein (200 μg/mL),[26] and wortmannin (100 μM).[44] The cells were washed with PBS three times, 0.4% trypan blue once and cracked.[27] The lysate was quantitatively determined by the fluorospectro photometer. All operations were conducted strictly away from light. The FITC-labeled materials were determined by MTT assay.

In Vitro Gene Silence. A siRNA sequence targeting the human VEGF gene was purchased from Shanghai Genepharma Co., Ltd. The sense and antisense sequences were 5′-GGAGUACCCUGAUGAGAUCdTdT-3′ and 5′-GAUCUCAUCAGGGUACUCCdTdT-3′, respectively. A negative control (NC) sequence (5′-UUCUCCGAACGUGUCACGUdTdT-3′, 5′-ACGUGACACGUUCGGAGAAdTdT-3′) was used as control. The test was conducted as the gene transfection assay with the difference of gene complexes and evaluation methods. The copolymers/siRNA complexes were prepared at each optimal transfection weight ratio (referring to pDNA transfection) with 0.5, 1, 2.5, 5, 7.5 μg siRNA per sample. The gene silence efficiency was measured by MTT assay at 490 nm and Western blot (VEGF). Untreated and PEI/NC-siRNA treated cells served as negative control.

In Vivo Biodistribution. The tumor-bearing mice were intravenously injected BODIPY-labeled mPEG-SS-Lys_{95}-r-His_{20} (200 μg in 150 μL PBS per mouse) and imaged by the Maestro IN-VIVO imaging system (excitation at 589 nm, emission at 617 nm, CRI, MA) at 30 min, 1 h, 2 h, 4 h, and 24 h post injection.[45] Then, the mice were euthanized by cervical dislocation and taken out of the livers, spleens, lungs, kidneys, and tumors. The tissues were imaged in the same conditions. Fluorescence signal intensity of tissues was quantified by Maestro version 2.10.0.

In Vivo Transfection with pEGFP Reporter Plasmid. The tumor-bearing mice were injected mPEG-SS-Lys_{95}-r-His_{20}/pEGFP complexes (w/w = 2) via the tail vein. After 7 days, the mice were fixed by heart perfusion.[46] Then, the livers, spleens, lungs, kidneys, and tumors were dissected, subsided with gradient sucrose, embedded in OCT (Sakura, U.S.A.) and sectioned at 10 μm. The frozen slides were observed using CLSM. The mice treated with PBS were used as negative control.

In Vivo Antitumor Effect with VEGF-siRNA. Fifteen tumor-bearing mice were randomly assigned to 3 groups: PBS, mPEG-SS-Lys_{95}-r-His_{20}/VEGF-siRNA (w/w = 2, 20 μg siRNA) and mPEG-SS-Lys_{55}-r-His_{20}/VEGF-siRNA (w/w = 3, 20 μg siRNA). The mice were injected 150 μL PBS or complexes and recorded the body weight and tumor volume every other day for 3 weeks. At day 22, the tumors were collected, weighed, photographed and analyzed by Western blot. The tumor volume was calculated by the equation: $V = WL^2/2$, where W means the longest diameter and L means the shortest diameter.

Statistics Analysis. Data were analyzed with SPSS 17.0 using one-way analysis of variance (ANOVA) and SNK-q test and LSD test. The results were presented as mean ± standard deviation (SD). Statistical significance of the results was judged at $p < 0.05$.

■ ASSOCIATED CONTENT

Ⓢ Supporting Information

Additional data of optical microscope image, quantitative transfection efficiency, qualitative transfection effects, cytotoxicity, and in vivo distribution. This material is available free of charge via the Internet at http://pubs.acs.org.

■ AUTHOR INFORMATION

Corresponding Authors

*Email: yongyong_li@tongji.edu.cn.
*Email: sjs@tongji.edu.cn.

Author Contributions

‖Authors H.Y.Z. and C.Y.D. contributed equally to this work. The manuscript was written through contributions of all authors.

Notes

The authors declare no competing financial interest.

■ ACKNOWLEDGMENTS

This work was financially supported by 973 program (2013CB967500) and National Natural Science Foundation of China (51173136, 21104059, 81371949, and 30970726), Shanghai Rising-Star Program (12QA1403400), and "Chen Guang" project founded by Shanghai Municipal Education Commission and Shanghai Education Development Foundation.

■ REFERENCES

(1) Wang, T.; Upponi, J. R.; Torchilin, V. P. Design of Multifunctional Non-viral Gene Vectors to Overcome Physiological Barriers: Dilemmas and Strategies. *Int. J. Pharm.* **2012**, *427*, 3−20.

(2) Nimesh, S.; Gupta, N.; Chandra, R. Strategies and Advances in Nanomedicine for Targeted siRNA Delivery. *Nanomedicine* **2011**, *6*, 729−746.

(3) Mann, A.; Thakur, G.; Shukla, V.; Ganguli, M. Peptides in DNA Delivery: Current Insights and Future Directions. *Drug Discovery Today* **2008**, *13*, 152−160.

(4) Osada, K.; Kataoka, K. Drug and Gene Delivery Based on Supramolecular Assembly of PEG-Polypeptide Hybrid Block Copolymers. *Adv. Polym. Sci.* **2006**, *202*, 113−153.

(5) Scholz, C.; Wagner, E. Therapeutic Plasmid DNA Versus siRNA Delivery: Common and Different Tasks for Synthetic Carriers. *J. Controlled Release* **2012**, *161*, 554−565.
(6) Cai, X. J.; Dong, C. Y.; Dong, H. Q.; Wang, G. M.; Pauletti, G. M.; Pan, X. J.; Wen, H. Y.; Mehl, I.; Li, Y. Y.; Shi, D. L. Effective Gene Delivery Using Stimulus-Responsive Catiomer Designed with Redox-Sensitive Disulfide and Acid-Labile Imine Linkers. *Biomacromolecules* **2012**, *13*, 1024−1034.
(7) Cai, X.-J.; Dong, H.-Q.; Xia, W.-J.; Wen, H.-Y.; Li, X.-Q.; Yu, J.-H.; Li, Y.-Y.; Shi, D.-L. Glutathione-Mediated Shedding of PEG Layers Based on Disulfide-Linked Catiomers for DNA Delivery. *J. Mater. Chem.* **2011**, *21*, 14639−14645.
(8) Tuschl, T. RNA Interference and Small Interfering RNAs. *ChemBioChem* **2001**, *2*, 239−245.
(9) Haupenthal, J.; Baehr, C.; Kiermayer, S.; Zeuzem, S.; Piiper, A. Inhibition of Rnase a Family Enzymes Prevents Degradation and Loss of Silencing Activity of siRNAs in Serum. *Biochem. Pharmacol.* **2006**, *71*, 702−710.
(10) Janib, S. M.; Pastuszka, M.; Aluri, S.; Folchman-Wagner, Z.; Hsueh, P. Y.; Shi, P.; Yi, A.; Cui, H.; Mackay, J. A. A Quantitative Recipe for Engineering Protein Polymer Nanoparticles. *Polym. Chem.* **2014**, *5*, 1614−1625.
(11) Zhou, J. H.; Liu, J.; Shi, T.; Xia, Y. Q.; Luo, Y.; Liang, D. H. Phase Separation of siRNA−Polycation Complex and Its Effect on Transfection Efficiency. *Soft Matter.* **2013**, *9*, 2262−2268.
(12) Hong, W.; Zhang, R. H.; Di, Z. Y.; He, Y. W.; Zhao, Z. H.; Hu, J.; Wu, Y. L.; Li, W. X.; Cao, Z. J. Design of Histidine-Rich Peptides with Enhanced Bioavailability and Inhibitory Activity against Hepatitis C Virus. *Biomaterials* **2013**, *34*, 3511−3522.
(13) Pack, D. W.; Putnam, D.; Langer, R. Design of Imidazole-Containing Endosomolytic Biopolymers for Gene Delivery. *Biotechnol. Bioeng.* **2000**, *67*, 217−223.
(14) Gu, J.; Wang, X.; Jiang, X.; Chen, Y.; Chen, L.; Fang, X.; Sha, X. Self-Assembled Carboxymethyl Poly(L-histidine) Coated Poly(B-Amino Ester)/DNA Complexes for Gene Transfection. *Biomaterials* **2012**, *33*, 644−658.
(15) Asayama, S.; Sudo, M.; Nagaoka, S.; Kawakami, H. Carboxymethyl Poly(L-histidine) as a New pH-Sensitive Polypeptide to Enhance Polyplex Gene Delivery. *Mol. Pharmaceut.* **2008**, *5*, 898−901.
(16) Ihm, J.; Han, K.; Hwang, C.; Kang, J.; Ahn, K.; Han, I.; Han, D.; Hubbell, J.; Cho, C. Poly(4-vinylimidazole) as Nonviral Gene Carrier: In Vitro and In Vivo Transfection. *Acta Biomater.* **2005**, *1*, 165−172.
(17) Danielsen, S.; Varum, K. M.; Stokke, B. T. Structural Analysis of Chitosan Mediated DNA Condensation by AFM: Influence of Chitosan Molecular Parameters. *Biomacromolecules* **2004**, *5*, 928−936.
(18) Liu, Y. M.; Reineke, T. M. Hydroxyl Stereochemistry and Amine Number within Poly(Glycoamidoamine)s Affect Intracellular DNA Delivery. *J. Am. Chem. Soc.* **2005**, *127*, 3004−3015.
(19) Kurosaki, T.; Kitahara, T.; Fumoto, S.; Nishida, K.; Nakamura, J.; Niidome, T.; Kodama, Y.; Nakagawa, H.; To, H.; Sasaki, H. Ternary Complexes of PDNA, Polyethylenimine, and Γ-Polyglutamic Acid for Gene Delivery Systems. *Biomaterials* **2009**, *30*, 2846−2853.
(20) Kim, T.-i.; Kim, S. W. Bioreducible Polymers for Gene Delivery. *React. Funct. Polym.* **2011**, *71*, 344−349.
(21) Maruyama, K.; Iwasaki, F.; Takizawa, T.; Yanagie, H.; Niidome, T.; Yamada, E.; Ito, T.; Koyama, Y. Novel Receptor-Mediated Gene Delivery System Comprising Plasmid/Protamine/Sugar-Containing Polyanion Ternary Complex. *Biomaterials* **2004**, *25*, 3267−3273.
(22) Lu, B.; Xu, X. D.; Zhang, X. Z.; Cheng, S. X.; Zhuo, R. X. Low Molecular Weight Polyethylenimine Grafted N-Maleated Chitosan for Gene Delivery: Properties and In Vitro Transfection Studies. *Biomacromolecules* **2008**, *9*, 2594−2600.
(23) Goncalves, C.; Pichon, C.; Guerin, B.; Midoux, P. Intracellular Processing and Stability of DNA Complexed with Histidylated Polylysine Conjugates. *J. Gene. Med.* **2002**, *4*, 271−281.
(24) Kunath, K.; von Harpe, A.; Fischer, D.; Peterson, H.; Bickel, U.; Voigt, K.; Kissel, T. Low Molecular Weight Polyethylenimine as a Non-viral Vector for DNA Delivery: Comparison of Physicochemical Properties, Transfection Efficiency, and In Vivo Distribution with High Molecular Weight Polyethylenimine. *J. Controlled Release* **2003**, *89*, 113−125.
(25) Sanchez-San Martin, C.; Lopez, T.; Arias, C. F.; Lopez, S. Characterization of Rotavirus Cell Entry. *J. Virol.* **2004**, *78*, 2310−2318.
(26) He, C.; Yin, L.; Tang, C.; Yin, C. Multifunctional Polymeric Nanoparticles for Oral Delivery of Tnf-A siRNA to Macrophages. *Biomaterials* **2013**, *34*, 2843−2854.
(27) He, C.; Hu, Y.; Yin, L.; Tang, C.; Yin, C. Effects of Particle Size and Surface Charge on Cellular Uptake and Biodistribution of Polymeric Nanoparticles. *Biomaterials* **2010**, *31*, 3657−3666.
(28) Khalil, I. A.; Kogure, K.; Akita, H.; Harashima, H. Uptake Pathways and Subsequent Intracellular Trafficking in Nonviral Gene Delivery. *Pharmacol. Rev.* **2006**, *58*, 32−45.
(29) Kaksonen, M.; Toret, C. P.; Drubin, D. G. Harnessing Actin Dynamics for Clathrin-Mediated Endocytosis. *Nat. Rev. Mol. Cell Biol.* **2006**, *7*, 404−414.
(30) Li, W.; Szoka, F. C. Lipid-Based Nanoparticles for Nucleic Acid Delivery. *Pharm. Res.* **2007**, *24*, 438−449.
(31) Ke, W.; Shao, K.; Huang, R.; Han, L.; Liu, Y.; Li, J.; Kuang, Y.; Ye, L.; Lou, J.; Jiang, C. Gene Delivery Targeted to the Brain Using an Angiopep-Conjugated Polyethyleneglycol-Modified Polyamidoamine Dendrimer. *Biomaterials* **2009**, *30*, 6976−6985.
(32) Ding, Y.; Wang, W.; Feng, M.; Wang, Y.; Zhou, J.; Ding, X.; Zhou, X.; Liu, C.; Wang, R.; Zhang, Q. A Biomimetic Nanovector-Mediated Targeted Cholesterol-Conjugated siRNA Delivery for Tumor Gene Therapy. *Biomaterials* **2012**, *33*, 8893−8905.
(33) Wang, H.-Y.; Yi, W.-J.; Qin, S.-Y.; Li, C.; Zhuo, R.-X.; Zhang, X.-Z. Tyroserleutide-Based Gene Vector for Suppressing Vegf Expression in Cancer Therapy. *Biomaterials* **2012**, *33*, 8685−8694.
(34) Kumar, P.; Wu, H.; McBride, J. L.; Jung, K. E.; Kim, M. H.; Davidson, B. L.; Lee, S. K.; Shankar, P.; Manjunath, N. Transvascular Delivery of Small Interfering RNA to the Central Nervous System. *Nature* **2007**, *448*, 39−43.
(35) Kim, D.; Lee, E. S.; Oh, K. T.; Gao, Z. G.; Bae, Y. H. Doxorubicin-Loaded Polymeric Micelle Overcomes Multidrug Resistance of Cancer by Double-Targeting Folate Receptor and Early Endosomal pH. *Small* **2008**, *4*, 2043−2050.
(36) Ding, J.; Chen, J.; Li, D.; Xiao, C.; Zhang, J.; He, C.; Zhuang, X.; Chen, X. Biocompatible Reduction-Responsive Polypeptide Micelles as Nanocarriers for Enhanced Chemotherapy Efficacy In Vitro. *J. Mater. Chem. B* **2013**, *1*, 69−81.
(37) Kim, Y. Y.; Ganesan, K.; Yang, P. C.; Kulak, A. N.; Borukhin, S.; Pechook, S.; Ribeiro, L.; Kroger, R.; Eichhorn, S. J.; Armes, S. P.; Pokroy, B.; Meldrum, F. C. An Artificial Biomineral Formed by Incorporation of Copolymer Micelles in Calcite Crystals. *Nat. Mater.* **2011**, *10*, 890−896.
(38) Li, Y.-Y.; Hua, S.-H.; Xiao, W.; Wang, H.-Y.; Luo, X.-H.; Li, C.; Cheng, S.-X.; Zhang, X.-Z.; Zhuo, R.-X. Dual-Vectors of Anti-cancer Drugs and Genes Based on pH-Sensitive Micelles Self-Assembled from Hybrid Polypeptide Copolymers. *J. Mater. Chem.* **2011**, *21*, 3100−3106.
(39) Chu, M.; Dong, C. Y.; Zhu, H. Y.; Cai, X. J.; Dong, H. Q.; Ren, T. B.; Su, J. S.; Li, Y. Y. Biocompatible Polyethylenimine-Graft-Dextran Catiomer for Highly Efficient Gene Delivery Assisted by a Nuclear Targeting Ligand. *Polym. Chem.—U.K.* **2013**, *4*, 2528−2539.
(40) Pathak, A.; Kumar, P.; Chuttani, K.; Jain, S.; Mishra, A. K.; Vyas, S. P.; Gupta, K. C. Gene Expression, Biodistribution, and Pharmacoscintigraphic Evaluation of Chondroitin Sulfate-Pei Nanoconstructs Mediated Tumor Gene Therapy (Vol 3, p 1493, 2009). *ACS Nano* **2009**, *3*, 2854−2854.
(41) Lo, S. L.; Wang, S. An Endosomolytic Tat Peptide Produced by Incorporation of Histidine and Cysteine Residues as a Nonviral Vector for DNA Transfection. *Biomaterials* **2008**, *29*, 2408−2414.
(42) Florian, P.; Macovei, A.; Sima, L.; Nichita, N.; Mattsby-Baltzer, I.; Roseanu, A. Endocytosis and Trafficking of Human Lactoferrin in Macrophage-like Human Thp-1 Cells. *Biochem. Cell Biol.* **2012**, *90*, 449−455.

(43) Bertuccini, L.; Ammendolia, M.; Superti, F.; Baldassarri, L. Invasion of HeLa Cells by *Enterococcus faecalis* Clinical Isolates. *Med. Microbiol. Immun.* **2002**, *191*, 25−31.
(44) Guo, C. J.; Wu, Y. Y.; Yang, L. S.; Yang, X. B.; He, J.; Mi, S.; Jia, K. T.; Weng, S. P.; Yu, X. Q.; He, J. G. Infectious Spleen and Kidney Necrosis Virus (a Fish Iridovirus) Enters Mandarin Fish Fry Cells Via Caveola-Dependent Endocytosis. *J. Virol.* **2011**, *86*, 2621−2631.
(45) Han, L. A.; Li, J. F.; Huang, S. X.; Huang, R. Q.; Liu, S. H.; Hu, X.; Yi, P. W.; Shan, D.; Wang, X. X.; Lei, H.; Jiang, C. Peptide-Conjugated Polyamidoamine Dendrimer as a Nanoscale Tumor-Targeted T1Magnetic Resonance Imaging Contrast Agent. *Biomaterials* **2011**, *32*, 2989−2998.
(46) Qian, Y.; Zha, Y.; Feng, B.; Pang, Z.; Zhang, B.; Sun, X.; Ren, J.; Zhang, C.; Shao, X.; Zhang, Q.; Jiang, X. Pegylated Poly(2-(Dimethylamino) Ethyl Methacrylate)/DNA Polyplex Micelles Decorated with Phage-Displayed TGN Peptide for Brain-Targeted Gene Delivery. *Biomaterials* **2013**, *34*, 2117−2129.